Parallel Interleaved VSCs: Influence of the PWM Scheme on the Design of the Coupled Inductor

Ghanshyamsinh Gohil, Lorand Bede, RamKrishan Maheshwari, Remus Teodorescu, Tamas Kerekes, Frede Blaabjerg
Department of Energy Technology, Aalborg University, Denmark
gvg@et.aau.dk

***Abstract*—The line current ripple and the size of the dc-link capacitor can be reduced by interleaving the carriers of the parallel connected Voltage Source Converters (VSCs). However, the interleaving of the carriers gives rise to the circulating current between the VSCs, and it should be suppressed. To limit the circulating current, magnetic coupling between the interleaved legs of the corresponding phase is provided by means of a Coupled Inductor (CI). The design of the CI is strongly influenced by the Pulsewidth Modulation (PWM) scheme used. The analytical model to evaluate the flux-linkage in the CI is presented in this paper. The maximum flux density and the core losses, being the most important parameters for the CI design, are evaluated for continuous PWM and discontinuous pulsewidth modulation (DPWM) schemes. The effect of these PWM schemes on the design of the CI is discussed. The simulation and the experimental results are finally presented to validate the analysis.**

***Index Terms*—Voltage source converters (VSC), parallel, interleaving, coupled inductor, PWM**

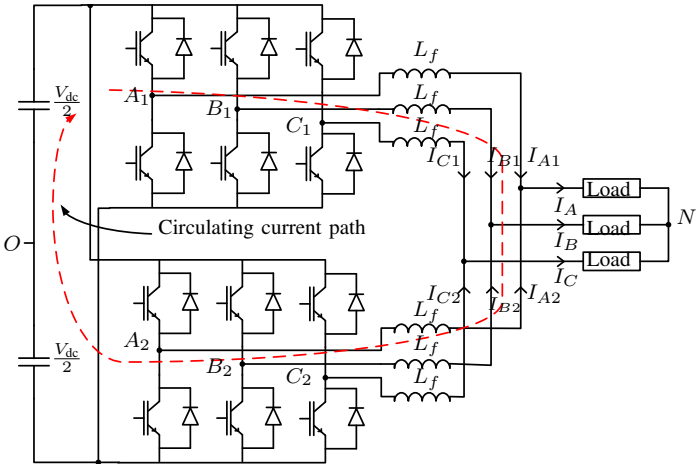

Fig. 1. Parallel interleaved VSCs with the common dc-link.

I. Introduction

The magnetic excitation in the core of the line filter inductor has a line frequency component along with the small high frequency ripple components. By improving the line current quality, a small filter and therefore higher power density can be achieved. The line current quality can be improved by interleaving the carrier signals of the parallel Voltage Source Converters (VSCs) [1]–[6]. The discussion on the optimal interleaving angle to minimize the line current ripple is presented in [2]. The optimized PulseWidth Modulation (PWM) scheme involving multiple sequences and different interleaving angles to reduce the line current ripple is also presented [6]. The zone division plot, showing the spatial regions within a sector where a combination of a certain switching sequence and interleaving angle result in lower rms current ripple in a switching cycle, is also discussed.

The interleaving of the carriers leads to the phase shifted pole voltages (measured with respect to the center point of the dc-link O in Fig. 1.) of the corresponding phases of the parallel interleaved VSCs. This gives rise to the circulating current between VSCs, and it should be limited in order to reduce the losses and the stresses in both active and passive components, present in the circulating current path. The magnetic coupling between the interleaved parallel legs, by means of a Couple Inductor (CI) is proposed in [7]–[10], and the schematic is shown in Fig. 2(a). To achieve high power density, the size of this additional circulating current filter should be reduced.

If a strong magnetic coupling between the windings is ensured, the CI is only subjected to high frequency magnetic excitation, which is determined by the switching frequency of the VSCs. As a result of the high frequency excitation, small size of the CI can be achieved. Moreover, the maximum value of the flux-density in the core should be close to the saturation flux density, in order to utilize the core effectively. High frequency flux reversal along with the high flux-density in the core results in more core losses. On the other hand, limited surface area is available for heat dissipation due to the small size of the CI. This may lead to a thermally limited design. As the core losses also depend on the peak flux density, the design of the thermally limited inductor can be realized by either decreasing the peak value of the flux density in the core or by providing more cooling. Both of these options lead to reduced power density.

The core losses depend on the peak flux density and the rate of change of flux density. Both of these parameters are strongly influenced by the PWM scheme used. The peak flux density in the core of the CI for different PWM schemes are discussed in [9], and a modulation scheme to reduce the flux in the CI is also proposed. However, discussion on the core losses is not given, which is an important factor in determining the size of the thermally limited magnetic component, and it should be considered carefully for a proper design of the CI.

The CI is a preferred solution for suppressing the circulating

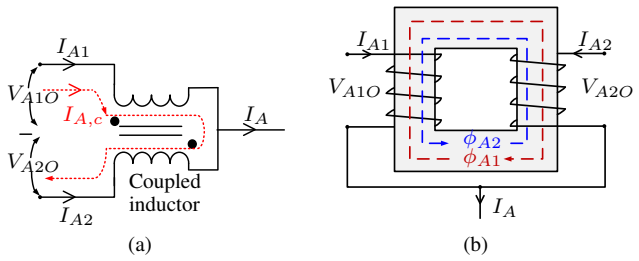

Fig. 2. Coupled inductor. (a) schematic for phase A, (b) physical arrangement of CI.

current in the parallel interleaved VSCs, and the effect of the carrier based PWM schemes on the design of the CI is analyzed in this paper. The core experiences high frequency excitation and therefore, small size of the CI can be achieved. However, due to the small size, the surface area available for the heat dissipation is limited. The effect of the PWM scheme on the parameters affecting the design of the CI is discussed. Moreover, an analytical method to evaluate the maximum flux-density and losses in the CI for different PWM schemes is presented. The basic operation of the CI is discussed in Section II. The effect of the PWM schemes on the flux density in the magnetic core of the CI is presented in Section III. The influence of the flux density pattern on the design of the CI is presented in Section IV. In Section VI, the simulation results and the experimental results are presented to validate the analysis.

II. Coupled Inductor

The instantaneous potential difference in the pole voltages of the interleaved phase of the parallel VSCs gives rise to the circulating current. The individual leg current (I_{A1} and I_{A2}) carries the circulating current in addition to the line current, and it can be decomposed into two components given as

$$\begin{aligned} I_{A1} &= I_{A1,l} + I_{A,c} \\ I_{A2} &= I_{A2,l} - I_{A,c} \end{aligned} \tag{1}$$

where, $I_{A1,l}$ and $I_{A2,l}$ are the components of the phase currents contributing to the resultant line current, and $I_{A,c}$ is the circulating current component. Assuming ideal VSCs and neglecting the effect of the hardware/control asymmetry, the current components contributing to the line current of the VSCs are considered equal. Therefore, the resultant line current is given as

$$I_A = 2I_{A1,l} = 2I_{A2,l}, \tag{2}$$

and the circulating current between the VSCs is given as

$$I_{A,c} = \frac{I_{A1} - I_{A2}}{2} \tag{3}$$

The magnetic coupling between the parallel interleaved legs provided by the CI is used to suppress the circulating current, as discussed below.

The schematic of the CI is shown in Fig. 2(a), and one of the possible physical arrangements of the CI is depicted in Fig. 2(b). The flux linkage in the CI is given as

$$\lambda_A(t) = \lambda_{A1}(t) + \lambda_{A2}(t) = \int (V_{A1O} - V_{A2O})dt \tag{4}$$

where V_{A1O} and V_{A1O} are the pole voltages measured with respect to the fictitious dc-link mid-point O, as shown in Fig. 1. The flux density in the core is given as

$$B_A(t) = \frac{1}{2NA_c} \int (V_{A1O} - V_{A2O})dt \tag{5}$$

where N is the number of turns and A_c is the core cross-sectional area. The maximum value of the flux density and the core losses are the important parameters to consider in the design of the CI. From (5), it can be inferred that the flux density depends on the time integral of the pole voltage differences, which in turn depends on the dc-link voltage, the interleaving angle,the modulation index, and the PWM scheme used. Therefore, the effect of the PWM schemes on the design of the CI is analyzed in the following section.

III. Pulsewidth Modulation Schemes and their Effect on the Coupled Inductor Design

The reference space vector $\vec{V}_{ref}$ is sampled, and it's magnitude (V_{ref}) and angle (ψ) information is used for the selection of the two adjacent active state vectors along with the zero vectors to synthesize the $\vec{V}_{ref}$ [11]–[13]. The respective dwell time of the active vectors is chosen to maintain the volt-sec balance. Let T_1, T_2, and T_z be the dwell times of the vectors $\vec{V}_1$, $\vec{V}_2$, and $\vec{V}_0/\vec{V}_7$, respectively, and it is given by

$$T_1 = \frac{2}{\sqrt{3}} \frac{|\vec{V}_{ref}|}{V_{\text{dc}}} T_s \sin(60° - \psi) \tag{6a}$$

$$T_2 = \frac{2}{\sqrt{3}} \frac{|\vec{V}_{ref}|}{V_{\text{dc}}} T_s \sin(\psi) \tag{6b}$$

$$T_z = T_s - T_1 - T_2 \tag{6c}$$

where V_{dc} sis the dc-link voltage and T_s is the switching cycle. The time during which the zero vector is applied can be written as

$$\begin{aligned} T_z &= K_z T_z + (1 - K_z) T_z \\ &\text{where, } 0 \leqslant K_z \leqslant 1 \end{aligned} \tag{7}$$

Different modulation possibilities exist with variation in the parameter K_z [12]. $K_z = 0.5$ results in a classical center aligned Space Vector Modulation (SVM). Similarly, sequences for Discontinuous PWM (DPWM) schemes can be generated by choosing the appropriate value of K_z. The SVM, DPWM1 (60°clamp), DPWM2 and DPWM3 (30°) clamp PWM schemes are considered for comparison [12]–[14].

A. The Center-aligned Space Vector Modulation

The opposite polarity zero vectors are applied at the same time for the duration of $T_z/4$. For low modulation indices, the dwell time of the zero vectors is dominant. As a result, the CI is subjected to more flux-linkage at low modulation indices. In a thermally limited CI design, the power density decreases

TABLE I
SVM: FLUX DENSITY DESCRIPTION IN A HALF SWITCHING CYCLE USING PIECEWISE LINEAR EQUATIONS

PWM scheme	Sub-sector	Peak flux density B_p	Flux density $B(t)$
SVM	$0° \leq \psi \leq 90°$	$B_p = \frac{V_{\rm dc}(T_z)}{8NA_c}$	$B(t) = \frac{4B_p}{T_z}t$ for $0 \leq t \leq \frac{T_z}{4}$ $B(t) = B_p$ for $\frac{T_z}{2} \leq t \leq (\frac{T_s}{2} - \frac{T_z}{4})$ $B(t) = B_p - \frac{4B_p}{T_z}[t - (\frac{T_s}{2} - \frac{T_z}{4})]$ for $(\frac{T_s}{2} - \frac{T_z}{4}) \leq t \leq \frac{T_s}{2}$

TABLE II
DPWM1: FLUX DENSITY DESCRIPTION IN A HALF SWITCHING CYCLE USING PIECEWISE LINEAR EQUATIONS

Sub-sector	$\vec{V}_{ref}$ position	Peak flux density B_p	Flux density $B(t)$
$0° \leq \psi \leq 30°$	-	$B_p = 0$	$B(t) = 0$
$30° \leq \psi \leq 60°$	$M\cos(30° - \psi) \geqslant \frac{1}{\sqrt{3}}$	$B_p = \frac{V_{\rm dc}T_z}{4NA_c}$	$B(t) = \frac{-2B_p}{T_z}t$, for $0 \leq t \leq \frac{T_z}{2}$ $B(t) = -B_p$, for $\frac{T_z}{2} \leq t \leq \frac{T_s - T_z}{2}$ $B(t) = -B_p + \frac{2B_p}{T_z}[t - (\frac{T_s - T_z}{2})]$, for $\frac{T_s - T_z}{2} \leq t \leq \frac{T_s}{2}$
	$M\cos(30° - \psi) < \frac{1}{\sqrt{3}}$	$B_p = \frac{V_{\rm dc}(T_1+T_2)}{4NA_c}$	$B(t) = \frac{-2B_p}{T_1+T_2}t$, for $0 \leq t \leq \frac{T_1+T_2}{2}$ $B(t) = -B_p$, for $\frac{T_1+T_2}{2} \leq t \leq \frac{T_s - T_1 + T_2}{2}$ $B(t) = -B_p + \frac{2B_p}{T_1+T_2}[t - (\frac{T_s - T_1 - T_2}{2})]$, for $\frac{T_s - T_1 - T_2}{2} \leq t \leq \frac{T_s}{2}$
$60° \leq \psi \leq 90°$	$M\sin(60° - \psi_s) \geqslant \frac{1}{\sqrt{3}}$	$B_p = \frac{V_{\rm dc}(T_z+T_3)}{4NA_c}$	$B(t) = \frac{-2B_p}{T_z+T_3}t$, for $0 \leq t \leq \frac{T_z+T_3}{2}$ $B(t) = -B_p$, for $\frac{T_z+T_3}{2} \leq t \leq \frac{T_s - T_z - T_3}{2}$ $B(t) = -B_p + \frac{2B_p}{T_z+T_3}[t - (\frac{T_s - T_z - T_3}{2})]$, for $\frac{T_s - T_z - T_3}{2} \leq t \leq \frac{T_s}{2}$
	$M\sin(60° - \psi_s) \geqslant \frac{1}{\sqrt{3}}$	$B_p = \frac{V_{\rm dc}T_2}{4NA_c}$	$B(t) = \frac{-2B_p}{T_2}t$, for $0 \leq t \leq \frac{T_2}{2}$ $B(t) = -B_p$, for $\frac{T_2}{2} \leq t \leq \frac{T_s - T_2}{2}$ $B(t) = -B_p + \frac{2B_p}{T_z+T_3}[t - (\frac{T_s - T_2}{2})]$, for $\frac{T_s - T_2}{2} \leq t \leq \frac{T_s}{2}$

due to the high core losses as a result of the more flux-linkage at low modulation indices. The flux density pattern is identical in every quarter period of the fundamental cycle and can be described using piecewise linear equations as given in Table I. The asymmetrical regular sampled PWM scheme is considered [14]. Therefore, the peak flux-linkage $\lambda_{A,p}$ changes in every half switching cycle. As can be inferred from the flux density description given in Table I, the $\lambda_{A,p}$ is a function of the modulation index M and the reference space vector angle ψ. The maximum value of the peak flux-linkage as a function of modulation index is given as

$$\lambda_A, pmax = \frac{1}{4}V_{\rm dc}T_s \tag{8}$$

Although the maximum value of the peak flux-linkage is the same for all modulation indices, the flux-linkage pattern is different. The flux density in the CI for different modulation indices is shown in Fig. 3. The peak flux density in each half switching cycle is higher for lower modulation indices and reduces with the increase in the modulation index as evident from Fig. 3.

B. DPWM1: 60°Clamp

In most grid connected application, the grid current has a power factor close to unity and the use of the 60° clamp PWM (DPWM1) results in low switching loss reduction [11], [13], [15]. The non-switching interval for each phase leg is arranged around the positive and negative peaks of the respective reference voltage. The switching losses are reduced since each phase leg is not switched in a region where the current through the semiconductor devices of that leg is at its maximum value [14].

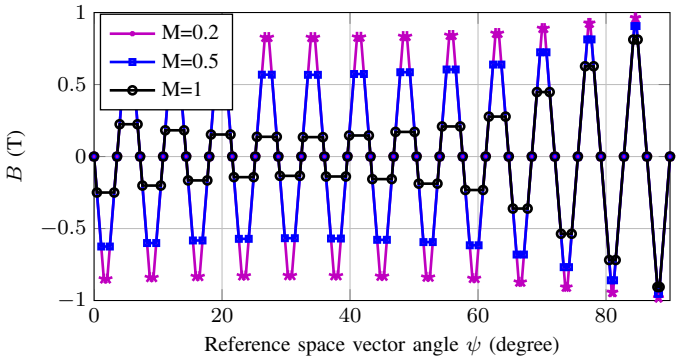

Fig. 3. The flux density in the CI when VSCs are modulated using SVM. The switching frequency is 2.5 kHz and maximum flux density in the core is restricted to 1 T.

The flux density in the CI depends on the magnitude and angle of the reference space vector $\vec{V}_{ref}$. The flux density in the CI for DPWM1 can be described using piecewise linear equations as given in Table II. The flux density for the first quarter of the fundamental cycle is plotted in Fig. 4 for modulation indices of 0.2, 0.5, and 1. The maximum peak flux-linkage varies with the modulation index, and it is given as

$$\lambda_{A,pmax} = \begin{cases} V_{\rm dc}T_s(\frac{1}{\sqrt{3}}\frac{|\vec{V}_{ref}|}{V_{\rm dc}}), & 0 \leq M < 1/\sqrt{3} \\ \frac{1}{4}V_{\rm dc}T_s, & 1/\sqrt{3} \leq M < 2/\sqrt{3} \end{cases} \tag{9}$$

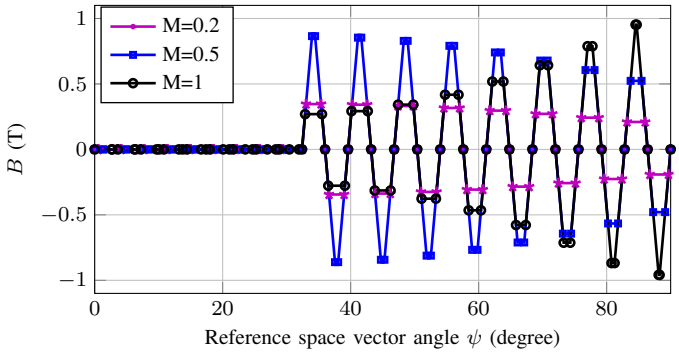

Fig. 4. The flux density in the CI core when DPWM1 is used. The switching frequency is 2.5 kHz and maximum flux density in the core is restricted to 1 T.

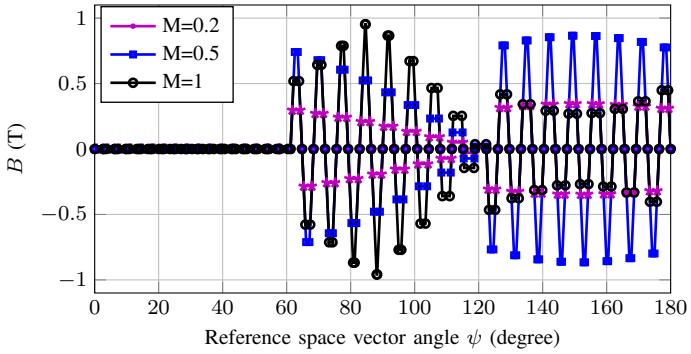

Fig. 5. The flux density in the CI core when DPWM2 is used. The switching frequency is 2.5 kHz and maximum flux density in the core is restricted to 1 T.

For modulation indices less than $1/\sqrt{3}$, the maximum value of the peak flux density in case of DPWM1 is less than that of the SVM. However, for a modulation indices higher than $1/\sqrt{3}$, the $\lambda_{A,pmax}$ for DPWM1 is the same as that of the SVM.

C. DPWM2: 30°Lagging Clamp

For a lagging power factor load, the use of DPWM2 can results in low switching losses [16]. Due to the asymmetrical switching sequence in each subsector, the flux density pattern is no longer identical in a quarter period of the fundamental cycle. Instead, the flux-density pattern is identical in every half period of the fundamental cycle. Similarly to DPWM1, the flux density in the CI for the DPWM2 can be also described by the piecewise linear equations. The flux density variation for different values of the modulation indices is plotted in Fig. 5. The maximum value of the peak flux density $\lambda_{A,pmax}$ is the same as that of the DPWM1, and can be described by (9).

D. DPWM3: 30°Clamp

In this PWM scheme, each phase leg is clamped to the opposite dc-link in each 60°segment. Different zero vectors are applied in each subsector (half of a 60°sector). The flux density pattern is plotted in Fig. 6. The peak flux-density

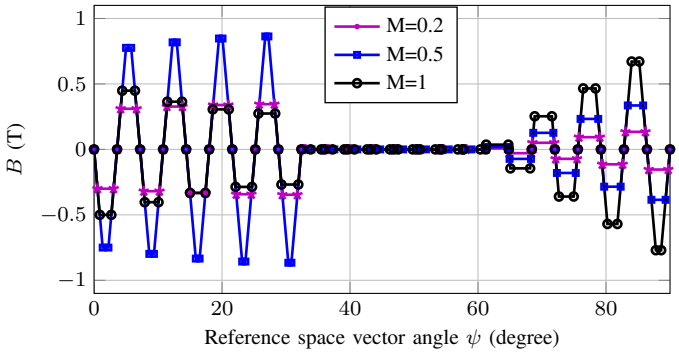

Fig. 6. The flux density in the CI core when DPWM3 is used. The switching frequency is 2.5 kHz and maximum flux density in the core is restricted to 1 T.

$\lambda_{A,pmax}$ is given as

$$\lambda_{A,pmax} = \begin{cases} V_{\rm dc}T_s(\frac{1}{\sqrt{3}}\frac{|\vec{\boldsymbol{V}}_{\boldsymbol{ref}}|}{V_{\rm dc}}), \\ \qquad \text{for } 0 \le M < 1/\sqrt{3} \\ \frac{1}{4}V_{\rm dc}T_s, \\ \qquad \text{for } 1/\sqrt{3} \le M < 2/3 \\ V_{\rm dc}T_s(\frac{1}{2} - \frac{1}{2}\frac{|\vec{\boldsymbol{V}}_{\boldsymbol{ref}}|}{V_{\rm dc}}), \\ \qquad \text{for } 2/3 \le M < 4/(3+\sqrt{3}) \\ V_{\rm dc}T_s(\frac{1}{2\sqrt{3}}\frac{|\vec{\boldsymbol{V}}_{\boldsymbol{ref}}|}{V_{\rm dc}}), \\ \qquad \text{for } 4/(3+\sqrt{3}) \le M < 2/\sqrt{3} \end{cases} \tag{10}$$

The CI suppresses the circulating current by providing magnetic coupling between the interleaved parallel legs. Assuming strong magnetic coupling between the windings, the flux in the core has only high frequency components, which are concentrated around the odd multiple of the carrier frequency. The high frequency excitation could lead to significant size reduction of the CI. However, more losses due to the high frequency excitation may result into increased loss density, and considerable thermal management is required [17], [18]. In order to achieve higher power density, active cooling is preferred [17]. However, active cooling increases complexity and should be avoided.

The size of the CI can also be reduced by operating with high flux density. However, this also results in increased losses. Thus, the volume optimized design of the CI may result in thermally limited design, where the maximum flux density in the core is determined by the heat dissipation capability of the CI [19], and not by the saturation flux density. For parallel interleaved VSCs, the PWM scheme has a strong influence on the maximum value of the peak flux density and the losses in the CI. The variation in the maximum value of the peak flux-linkage with the modulation index for different PWM schemes [9] is plotted in Fig. 7. The maximum value of the peak flux linkage is the same in all schemes. However, the flux-linkage pattern is different. As a result, the core losses would be different in each of the schemes, which is an important factor in determining the size and the efficiency of the CI, and it is discussed below.

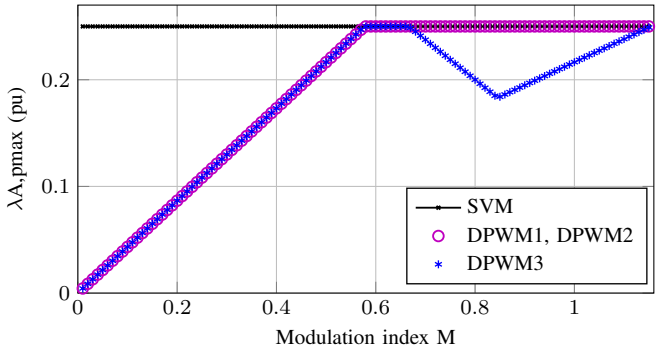

Fig. 7. The maximum peak flux linkage $\lambda_{A,pmax}$ variation with the modulation index. The flux-linkage is normalized with respect to the $V_{dc}T_s$.

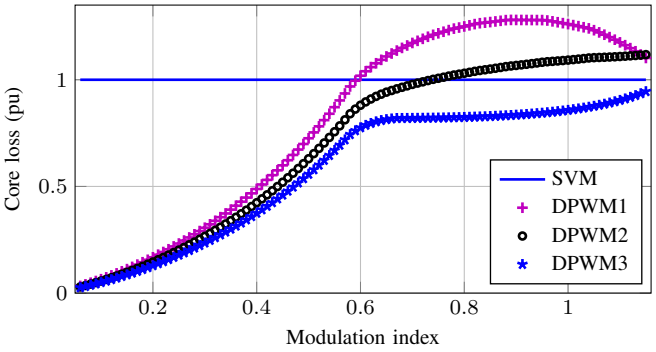

Fig. 8. The core losses in the CI for different PWM schemes. The core losses are normalized with respect to that of the SVM. The carrier frequency is taken to be the same in all cases.

The $\vec{V}_{ref}$ is sampled twice in a switching cycle, and the losses are evaluated for every half switching cycle. The flux density behavior in the half switching cycle can be described by the piecewise linear equations given in Table I and II for the SVM, and the DPWM1, respectively.

The Improved Generalized Steinmetz Equation (IGSE) [20], [21] is used to calculate the core losses, and the core losses per unit volume is given as

$$P_v = \frac{1}{T}\int_0^T k_i \left|\frac{dB(t)}{dt}\right|^{\alpha} (\Delta B)^{\beta-\alpha} dt \tag{11}$$

where α, β and k_i are the constants determined by the material characteristics. The flux density pattern is identical over a quarter period of the fundamental cycle. Therefore, the core losses are evaluated for each half switching cycle over a quarter period of the fundamental cycle. The average core loss over this period is given as

$$P_v = \frac{2}{(\frac{f_{sw}}{f_0})} \sum_{k=1}^{(\frac{f_{sw}}{2f_0})} \frac{2}{T_s} \int_0^{\frac{T_s}{2}} k_i (4B_{max} f_{sw})^{\alpha} (\Delta B_k)^{\beta-\alpha} dt \tag{12}$$

where f_0 is the fundamental frequency and f_{sw} is the switching frequency. The amorphous metal cores are considered, where the Steinmetz constants are $\alpha = 1.51$, $\beta = 1.74$ and $k_i = 0.622$.

To compare the PWM method independent of the design parameters, the volumetric losses in each of the DPWM schemes are normalized with respect to that of the SVM. From Fig. 8, it is evident that the DPWM3 outperforms other schemes in terms of the core losses. All the DPWM schemes have lower core losses compared to SVM at low modulation indices. The switching sequences involved in the DPWM2 are the same as the switching sequences of the DPWM1 in subsector 1 ($0° < \psi \leqslant 30°$) and switching sequences of DPWM3 in subsector 2 ($30° < \psi \leqslant 60°$). Thus, the core losses of the DPWM2 is an average of the core losses of the DPWM1 and core losses of the DPWM3 as depicted in Fig. 8. For high modulation indices, the DPWM1 has the highest core losses, followed by the DPWM2 and SVM.

TABLE III
PARAMETERS FOR SIMULATION STUDY

Parameters	Simulation study
Switching frequency	2.5 kHz
DC-link voltage	680 V
Maximum flux density B_{max}	1 T
Window utilization factor K_w	0.5
RMS current in winding $I_{A,1(rms)}$	8 A
Current density J	2 A/m^2
Core material	Amorphous metal AMCC40
Core cross-sectional area A_c	$3.7\times10^{-4} m^2$
No. of turns N	92

IV. Simulation and Experimental Results

The CI is designed using area a product approach and the design data are given in Table III. The area-product (A_p), which is the product of core cross-sectional area A_c and window area A_w, is given as

$$A_p = A_c \times A_w = \frac{V_{dc,max} I_{A,1(rms)}}{4K_w J B_{max} F_s} \tag{13}$$

where $V_{dc,max}$ is the maximum dc-link voltage, $I_{A,1(rms)}$ is the rms current flowing through each winding, K_w is the window utilization factor and B_{max} is the maximum flux density. The magnetic model is implemented in PLECS and the simulated flux density is depicted in Fig. 9. The flux density pattern for all PWM schemes closely matches with the analysis presented in Section III. The flux density and the circulating current for the SVM is plotted in Fig. 9(a) and 9(b), respectively. The simulation results are obtained with the modulation index of M=1. The core is excited only for two third period of the fundamental cycle for all DPWM schemes as evident from Fig. 9. The maximum value of the peak flux density in the CI is the same in all the PWM schemes with M=1 except for the DPWM3. The DPWM3 has a low value of the maximum flux density for high modulation indices, as shown in Fig. 7. The circulating current is proportional to the flux density in the core as it is evident from the Fig. 9(a) and 9(b), and thus the circulating current is measured and used for comparison of the PWM schemes in the experimental setup due to the ease of the measurement.

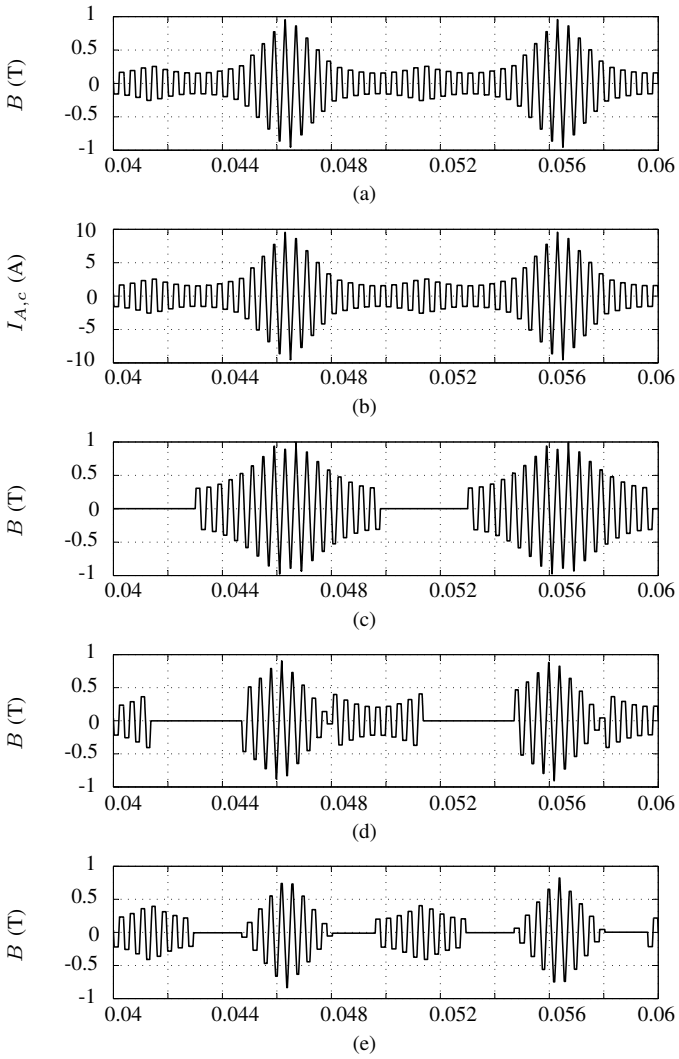

Fig. 9. Simulated flux density in the CI and the circulating current. (a) SVM: flux density, (b) SVM: circulating current, (c) DPWM1: flux density, (d) DPWM2: flux density, (e) DPWM3: flux density.

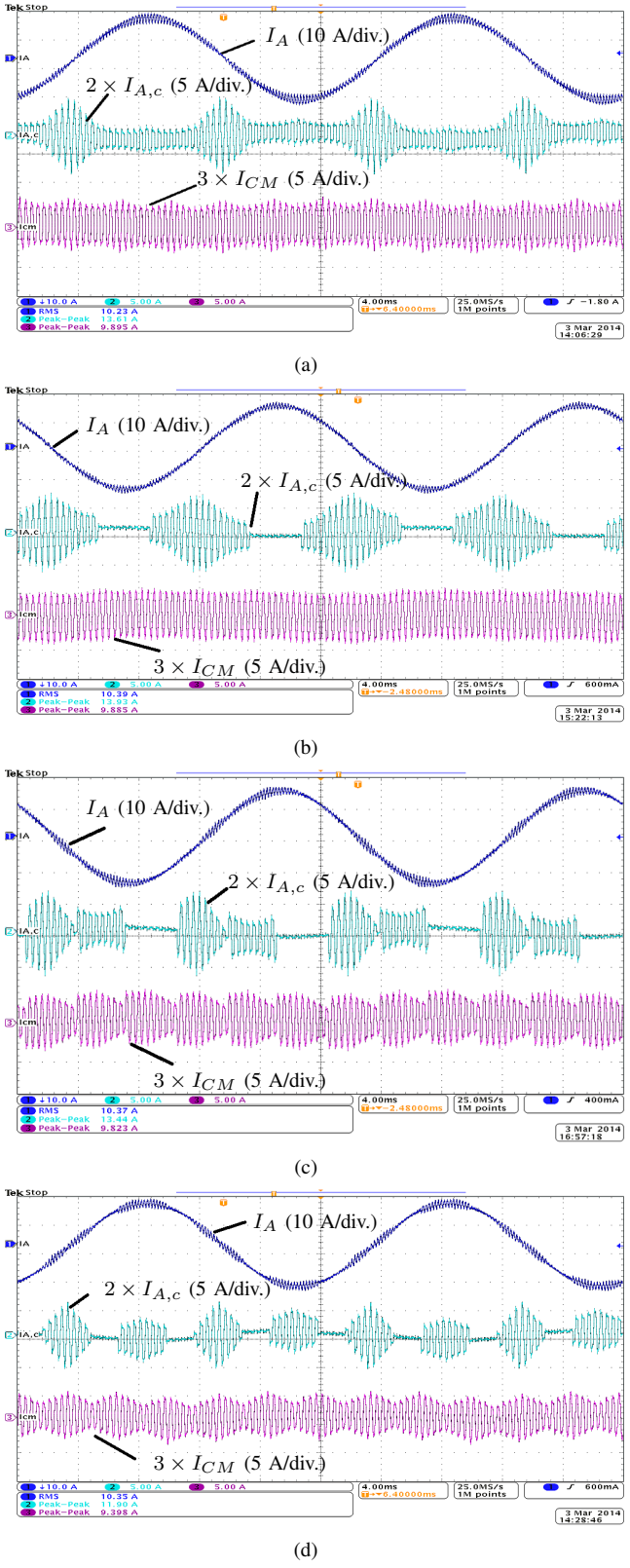

Fig. 10. Performance comparison of the PWM schemes: The modulation index M=1. (a) SVM, (b) DPWM1, (c) DPWM2, (d) DPWM3.

Experimental measurements have been obtained to demonstrate the validity of the analysis presented in the paper. The schematic of the test setup is shown in Fig. 1. The single phase inductors are used which will also introduce inductance in the circulating current path. This arrangement is adopted to simplify the measurement [9]. From Fig. 1, the dynamic behavior of the circulating current is given as

$$I_{A,c} = \frac{1}{2L_f} \int (V_{A1O} - V_{A2O})\, dt \tag{14}$$

From (4) and (14), it is clear that the circulating current ($I_{A,c}$) is a replica of the flux linkage in the core. Therefore, the measurements of $I_{A1} - I_{A2}$, which is equal to $2 \times I_{A,c}$ are obtained.

The dc-link voltage is set to 600 V. The carrier frequency is taken to be 2.5 kHz and the interleaving angle of 180°is chosen. The dead-time of 2 µs is used. The line filter inductor of 6.8 mH is used, and a resistive load is set to 20 Ω. The inductance in the circulating current path is 2×6.8 mH. The

results for modulation index of 1 for different PWM schemes are given in Fig. 10.

The maximum value of the peak circulating current $I_{A,c}$ is measured for different the PWM schemes. The modulation index is varied in the full linear range. The peak value of circulating current is different in each half switching period and the highest value of the peak of $I_{A,c}$ is captured and given in Table IV. The circulating current is a replica of the flux-linkage in the CI. The maximum value of the peak of the circulating current is the same for all of the PWM schemes. For SVM, a constant value of $I_{A,cmax}$ is observed over the entire modulation range, which is in agreement with the analysis presented in Section III. The DPWM schemes have smaller $I_{A,cmax}$ for lower modulation indices, and the $I_{A,cmax}$ variation with modulation index matches with the analysis.

TABLE IV
COMPARISON: MAXIMUM VALUE OF PEAK OF $I_{A,c}$ (A)

M	$I_{A,cmax}$			
	SVM	DPWM1	DPWM2	DPWM3
0.1	3.55	0.79	0.81	0.84
0.2	3.52	1.46	1.47	1.47
0.3	3.50	2.09	2.07	2.02
0.4	3.55	2.68	2.67	2.63
0.5	3.50	3.23	3.19	3.20
0.6	3.48	3.72	3.72	3.79
0.7	3.48	3.63	3.63	3.71
0.8	3.42	3.55	3.42	3.27
0.9	3.40	3.50	3.42	2.82
1.0	3.40	3.48	3.36	2.97
1.1	3.36	3.48	3.36	3.24
1.15	3.38	3.39	3.37	3.37

V. CONCLUSION

The influence of the PWM schemes on the design of the CI, used for the circulating current reduction in the parallel interleaved VSCs, is discussed. The carrier interleaving improves the line current quality, thus the size of the line filter can be reduced. However, it requires additional circulating current filter. The design of this filter is strongly influenced by the PWM scheme used. The analytical model to evaluate the flux density in the CI is presented. The maximum value of the peak flux density for different PWM schemes is the same, however the flux density pattern is different. This would results in different core losses. The core losses, being an important factor for proper thermal design of the CI, it is also evaluated for each of the PWM schemes. The use of the SVM results in high core losses for low modulation indices. The comparison also indicates that the use of DPWM3 results in the lowest core losses in the CI. Although the core is excited for two third period of the fundamental cycle in all DPWM schemes, the switching sequences involved in DPWM1 results in more flux linkage at high modulation indices and thus incurs the highest core losses for modulation indices higher than 0.6.

REFERENCES

[1] L. Asiminoaei, E. Aeloiza, P. N. Enjeti, and F. Blaabjerg, "Shunt active-power-filter topology based on parallel interleaved inverters," *IEEE Trans. Ind. Electron.*, vol. 55, no. 3, pp. 1175–1189, 2008.

[2] J. Prasad and G. Narayanan, "Minimization of Grid Current Distortion in Parallel-Connected Converters Through Carrier Interleaving," *IEEE Trans. Ind. Electron.*, vol. 1, no. c, pp. 1–1, 2013.

[3] S. Miller, T. Beechner, and J. Sun, "A comprehensive study of harmonic cancellation effects in interleaved three-phase vscs," in *Proc. IEEE Power Electronics Specialists Conference, 2007. PESC 2007.*, 2007, pp. 29–35.

[4] D. Zhang, F. Wang, R. Burgos, L. Rixin, and D. Boroyevich, "Impact of Interleaving on AC Passive Components of Paralleled Three-Phase Voltage-Source Converters," *IEEE Trans. Power Electron.*, vol. 46, no. 3, pp. 1042–1054, 2010.

[5] T. Bhavsar and G. Narayanan, "Harmonic analysis of advanced bus-clamping pwm techniques," *IEEE Trans. Power Electron.*, vol. 24, no. 10, pp. 2347–2352, 2009.

[6] X. Mao, A. Jain, and R. Ayyanar, "Hybrid interleaved space vector pwm for ripple reduction in modular converters," *IEEE Trans. Power Electron.*, vol. 26, no. 7, pp. 1954–1967, 2011.

[7] R. Hausmann and I. Barbi, "Three-phase multilevel bidirectional dc-ac converter using three-phase coupled inductors," in *Proc. IEEE Energy Conversion Congress and Exposition, 2009. ECCE 2009.*, Sept 2009, pp. 2160–2167.

[8] F. Forest, E. Laboure, T. Meynard, and V. Smet, "Design and comparison of inductors and intercell transformers for filtering of pwm inverter output," *IEEE Trans. Power Electron.*, vol. 24, no. 3, pp. 812–821, 2009.

[9] B. Cougo, T. Meynard, and G. Gateau, "Parallel Three-Phase Inverters: Optimal PWM Method for Flux Reduction in Intercell Transformers," *IEEE Trans. Power Electron.*, vol. 26, no. 8, pp. 2184–2191, Aug. 2011.

[10] B. Cougo, G. Gateau, T. Meynard, M. Bobrowska-Rafal, and M. Cousineau, "PD modulation scheme for three-phase parallel multi-level inverters," *IEEE Trans. Ind. Electron.*, vol. 59, no. 2, pp. 690–700, 2012.

[11] J. Kolar, H. Ertl, and F. C. Zach, "Influence of the modulation method on the conduction and switching losses of a pwm converter system," *IEEE Trans. Ind. Appl.*, vol. 27, no. 6, pp. 1063–1075, 1991.

[12] V. Blasko and V. Kaura, "A novel control to actively damp resonance in input lc filter of a three-phase voltage source converter," *IEEE Trans. Ind. Appl.*, vol. 33, no. 2, pp. 542–550, Mar 1997.

[13] A. Hava, R. Kerkman, and T. Lipo, "A high-performance generalized discontinuous pwm algorithm," *IEEE Trans. Ind. Appl.*, vol. 34, no. 5, pp. 1059–1071, 1998.

[14] D. G. Holmes and T. A. Lipo, *Pulse Width Modulation for Power Converters: Principles and Practice*. Hoboken, NJ: Wiley-IEEE Press, 2003.

[15] M. Depenbrock, "Pulse width control of a 3-phase inverter with nonsinusoidal phase voltages," in *Conf. Rec. IEEE Int. Semiconductor Power Conversion Conference*, 1997, pp. 399–403.

[16] A. Hava, R. Kerkman, and T. Lipo, "Simple analytical and graphical methods for carrier-based pwm-vsi drives," *IEEE Trans. Power Electron.*, vol. 14, no. 1, pp. 49–61, Jan 1999.

[17] G. Ortiz, J. Biela, and J. Kolar, "Optimized design of medium frequency transformers with high isolation requirements," in *Proc. 36th Annual Conference on IEEE Industrial Electronics Society, IECON 2010*, Nov 2010, pp. 631–638.

[18] R. Wrobel and P. Mellor, "Thermal design of high-energy-density wound components," *IEEE Trans. Ind. Electron.*, vol. 58, no. 9, pp. 4096–4104, Sept 2011.

[19] A. V. d. Bossche and V. C. Valchev, *Inductors and Transformers for Power Electronics*. Boca Raton, FL: CRC Press, 2004.

[20] K. Venkatachalam, C. Sullivan, T. Abdallah, and H. Tacca, "Accurate prediction of ferrite core loss with nonsinusoidal waveforms using only steinmetz parameters," in *Computers in Power Electronics, 2002. Proceedings. 2002 IEEE Workshop on*, 2002, pp. 36–41.

[21] J. Li, T. Abdallah, and C. Sullivan, "Improved calculation of core loss with nonsinusoidal waveforms," in *Industry Applications Conference, 2001. Thirty-Sixth IAS Annual Meeting. Conference Record of the 2001 IEEE*, vol. 4, 2001, pp. 2203–2210 vol.4.